RSC Advances

ROYAL SOCIETY OF CHEMISTRY

www.rsc.org/advances

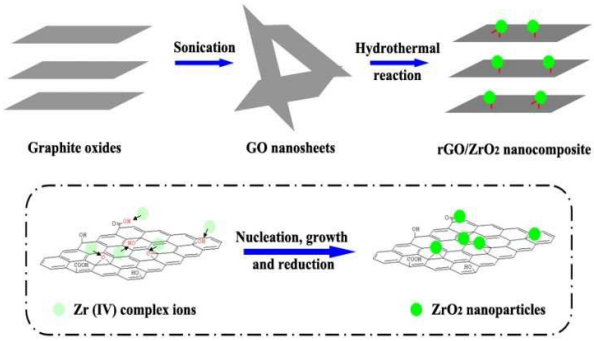

The schematic view for formation of rGO/ZrO_2 nanocomposite in hydrothermal reaction.

Preparation of reduced graphene oxide/zirconia nanocomposite and its application as a novel lubricant oil additive

Qi Zhou [a], Jingxia Huang [a], Jinqing Wang [b,*], Zhigang Yang [b], Sheng Liu [c], Zhaofeng Wang [b,*], and Shengrong Yang [b]

[a] College of Materials Science and Engineering, Lanzhou University of Technology, Lanzhou, 730050, P. R. China.

[b] State Key Laboratory of Solid Lubrication, Lanzhou Institute of Chemical Physics, Chinese Academy of Sciences, Lanzhou, 730000, P. R. China.

[c] The Technical Center of Zibo Entry-exit Inspection and Quarantine Bureau, Zibo 255031, P. R. China

Abstract:

The nanocomposites consisted of zirconia (ZrO_2) nanoparticles and the reduced graphene oxide (rGO) nanosheets were successfully fabricated by a one-pot hydrothermal method. By regulating proportion of the precursors of GO colloidal suspension and zirconium oxychloride ($ZrOCl_2$) solution, ZrO_2 nanoparticles with diameter of about 5 nm were uniformly anchored onto the rGO nanosheets. The combination mechanism of ZrO_2 nanoparticles fully bonded onto rGO nanosheets is the formation of the monodentate or bidentate composites between the containing-oxygen groups of GO and Zr(IV) complex ions from hydrolysis of $ZrOCl_2$

* Corresponding authors.

Tel./Fax: +86 931 4968076. E-mail addresses: jqwang@licp.cas.cn (J. Q. Wang), zhfwang@ licp.cas.cn (Z. F.Wang)

solution. The dispersibility and tribological properties of the prepared composites were investigated as novel lubricant additive in paraffin oil. The results suggested that the oil with a small amount of nanocomposite (0.06 wt%) exhibit the good dispersibility, excellent friction-reduction and anti-wear properties as well as the high load-bearing capacity caused by the synergistic effect of rGO nanosheets and ZrO_2 nanoparticles.

1. Introduction

In recent years, nanostructured carbon materials, such as carbon fiber, carbon nanotubes, fullerenes, etc, gained rapid development and widespread application due to their high load-bearing capacity and the chemical stability, low surface energy, weak intermolecular and strong intramolecular bonding. Moreover, these materials showed good tribological properties when they were used as lubricating materials. For instance, Hao *et al.*[1] reported that the multi-walled carbon nanotubes (MWCNTs) grafted with polyacrylamide as an additive in water exhibited good anti-wear and friction-reducing properties as well as the high load-carrying capacity. However, the desirable results were only achieved when the surface functionalization of CNT was performed by tedious and appropriate post-growth. In addition, Campbell *et al.*[2] observed the tribological properties of C_{60} molecules dissolved in dry toluene, the result showed that it had good load-bearing capacity attributing to the fact that the spherical fullerenes behaved as nanoscale ball bearings, but the effect was not obvious by comparison with macroscopic friction measurements.

Graphene, a two-dimensional carbon structure arranged in a honeycomb lattice, has attracted great attention of scientists since its discovery in 2004[3], owing to its remarkable electronic, optical, mechanical, thermal properties, high surface area and low density as well as ease to functionalization[4,5]. These features of graphene materials led to a broad range of potential applications in many areas, such as reinforced materials, hydrogen storage materials, nanoscale electronic devices, field-effect transistors and electrochemistry field[6]. In particular, graphene also has the formidable mechanical properties, with a high Young's modulus up to 1 TPa and a breaking strength of 130 GPa[7], it also exhibited high-efficient anti-wear and friction-reducing performances when used as a novel lubricating material[8,9]. Therefore, the tribological property of graphene is also of interest for application in micro/nano-electromechanical system except for its excellent electronic and mechanical properties[10]. For instance, Elomaa *et al.*[11] investigated the friction and wear performances of water as lubricant solvent containing 1 wt% of graphene oxide (GO) under a normal load of 10 N and the results showed that the friction coefficient decreased 57% compared to pure water. Berman *et al.*[12] demonstrated that graphene dispersed in ethanol could reduce the friction greatly but was instantly removed from the sliding surface under an applied load of 5 N.

It is well known that graphene has outstanding tribological properties, but its high surface energy induces the easy agglomeration, resulting in the poor dispersibility. It's lucky that the situation can be improved by surface modification of graphene, but most methods are organic-grafted. Mungse *et al.*[13] have synthesized

dual-layer alkylated graphene and used as lubricant additive, the result suggested that lube oils containing the alkylated graphene (0.02 mg/mL) exhibited a long-term dispersion stability, as well as the low friction and wear characteristics under the sliding contact between steel tribo-pairs. However, the organics usually are not environmentally friendly. Moreover, the lower hardness of graphene in the horizontal direction, and inevitable presences of defects and grain boundaries in macroscopic samples[14] have significant effect on widespread applications of graphene in tribological field.

Zirconia (ZrO_2) is one of the most important ceramic materials in the industry and has a potential applications to tribological field, attributing to its high mechanical strength, good chemical durability and thermal stability, and prominent tribological property as well as corrosion resistance and nontoxicity[15-17]. Over the past few years, researchers prepared graphene/ZrO_2 composites through different means; however these composites were mainly used in other fields, for examples, Shon *et al.*[18] demonstrated that graphene is an effective reinforcing agent to improve the mechanical properties of ZrO_2 composites. Rao *et al.*[19] synthesized surface modified graphene/ZrO_2 nanocomposite, which displayed excellent removal efficiency towards 4-chlorophenol from aqueous solution when used as the adsorbent. Salimi *et al.*[20] manifested that the reduced GO (rGO)/ZrO_2 nanocomposite exhibited the high performance as a novel architecture application to electrochemical sensing and biosensing platforms. Besides, Zheng *et al.*[21] synthesized graphene/ZrO_2 composite coatings using a plasma spraying technique and the results of wear test indicated that

the composite coatings exhibited excellent wear resistance and low friction coefficient. Therefore, preparation of composite consisted of ZrO_2 nanoparticles and rGO nanosheets, can not only satisfy these requirements of good lubricating properties and high load-bearing capacity, but also improve the dispersibility by anchoring ZrO_2 nanoparticles onto the surface of graphene to prevent the exfoliated rGO nanosheets from re-stacking.

Herein we introduce a simple and effective route to prepare the composite of rGO nanosheets homogeneously covered with ZrO_2 nanoparticles through adjusting the volume ratios of GO and zirconium oxychloride ($ZrOCl_2$) solutions; meanwhile, a possible mechanism for coating rGO nanosheets with ZrO_2 nanoparticles is also presented. Furthermore, the application of the prepared composite as lubricant additives has been investigated, and the results indicated that the tribological properties of the base oil of liquid paraffin could be improved by the addition of the composite under proper conditions, moreover, the possible friction-reduction and anti-wear mechanisms have also been discussed. To the best of our knowledge, no systematic studies have been covered about rGO/ZrO_2 nanocomposite as the lubricant additives even though graphene and its composites have been studied extensively in recent years.

2. Experimental section

2.1 Materials

All chemicals and reagents used in the experimental process are analytical grade, including graphite powder (≤30 μm), potassium persulfate ($K_2S_2O_8$, ≥99.5%),

phosphorus pentoxide (P_2O_5, ≥98.0%), sulfuric acid (H_2SO_4, 98%), potassium permanganate ($KMnO_4$, ≥99.5%), H_2O_2 (30 wt% in the water), hydrochloric acid (HCl, 36%~38%), zirconium oxychloride octahydrate ($ZrOCl_2·8H_2O$, ≥99.0%) and hydrazine hydrate ($N_2H_4·H_2O$, ≥80.0%). Besides, ultrapure water (>18 MΩcm) is used for preparation and rinsing.

2.2 Preparation of rGO/ZrO_2 composites

Expansible graphite powders were oxidized to graphite oxides using a modified Hummers method[22]. Subsequently, the as-prepared graphite oxides were exfoliated ultrasonically for 2 h to obtain the stable GO colloidal suspension. Then, rGO/ZrO_2 composites were synthesized by a simplified and high-efficient hydrothermal method similar to that described in the literature [20], in which GO colloidal suspension, $ZrOCl_2$ solution and $N_2H_4·H_2O$ were acted as rGO precursor, ZrO_2 precursor and reducing agent, respectively. In order to optimize the morphology of composites, a series of experiments were conducted by setting the mixed solutions of GO and $ZrOCl_2$ with different volume ratios (5:1, 3:1, 2:1, 1:1, 1:2). Firstly, GO colloidal suspension (2.33 mg/mL) and $ZrOCl_2$ solution (10 mM) were separately prepared and then mixed. After being sonicated for 30 min, 1 mL $N_2H_4·H_2O$ was added to the mixture (60 mL) of two solutions and sealed in a 100 mL autoclave and maintained at 180 °C for 18 h. The obtained black products were separated by centrifuging and washed with ultrapure water repeatedly, and freeze-dried for 12 h. For comparison, pure rGO and ZrO_2 were also prepared in the same way without the addition of $ZrOCl_2$ or GO and $N_2H_4·H_2O$.

2.3 Characterizations

The gross structural information and composition of samples were characterized by X-ray diffraction (XRD) analyses using Rigaku D/max-2400 X-ray diffractometer with Cu-Kα radiation (λ=0.154 nm) at 40kV and 150 mA in the range of 2θ=5 ~ 90°. The crystallite sizes were estimated using Debye-Scherrer formula. Further, the detailed microstructure, crystalline nature, and morphology characterizations of the as-synthesized samples were performed by transmission electron microscopy (TEM, FEI TECNAI G2 TF20) and high-resolution transmission electron microscopy (HRTEM), operated at 200 kV. Fourier transform infrared (FTIR) spectra for all samples were recorded on a Nicolet 380 FTIR spectrometer with a resolution of 0.125 cm^{-1}. Each sample in known quantity was mixed with potassium bromide (KBr) and prepared to the pellets for their FTIR measurements. All X-ray photoelectron spectroscopy (XPS) measurements were carried out on a PHI-5702 photoelectron spectrometer using an Al-Kα line as the X-ray source. Peak fitting of the C 1s and Zr 3d spectra for both samples were separately conducted using a Gaussian-Lorentzian function after performing a Shirley background correction.

2.4 Dispersible stability of rGO/ZrO_2 composite in paraffin

To evaluate the dispersion stability of rGO/ZrO_2 composite in base oil of liquid paraffin, the composite was ultrasonically dispersed in paraffin (with a density of about 0.8375 g/mL at 25 ℃ and the viscosities of 12.45 at 40 ℃ and 3.52 mm^2 /s at 100 ℃, respectively) for 1 h and then the homogeneous lubricant was obtained. For comparison, control samples including oil separately mixed with the pure ZrO_2,

graphite and rGO, have also been prepared in the same way. The concentration of these additives in paraffin was set as 0.06 wt% according to the results of friction test for the pure oil mixed with various concentrations of rGO/ZrO_2 composite. Dispersion stability of the composite and control samples in oil was investigated by means of absorbance measurement. Absorbance is measured by an ultraviolet-visible (UV-Vis) spectrophotometer using a UV-2600 spectrophotometer at set intervals. According to Bouguer-Lambert-Beer law, the absorbance is directly proportional to the concentration of solid particle in pure oil, which means that the higher absorbance is associated with the better dispersion stability of sample in the base oil. Moreover, photographs of the pure oil containing different additives were taken with different settling times for comparison.

2.5 Tribological properties of rGO/ZrO_2 nanocomposite as additive of paraffin oil

The tribological properties of the composites as lubricant additive were investigated at ambient temperature of around 25 °C and relative humidity of 25±5% by using SRV-4 reciprocating friction and wear tester (Optimal, Germany) with the testing method of ASTM D6425-05. The experiments were performed at loads of 50 ~ 450 N and a sliding speed of 6 cm/s, and the test duration of 30 min. The parameters were chosen to ensure boundary lubrication regime and simulate high load contact situations in components such as gears and bearings. The friction pairs were GCr15 bearing steel balls (φ = 10 mm, Ra =20 nm) and GCr15 bearing steel discs (24 mm × 8 mm). The hardness of the polished steel discs measured by MH-5-VM microhardness tester was 790~820 HV and the roughness of them determined by 3D

profilometer (NanoMap-D dual mode) was about 50 nm. To remove the surface organic contaminants of friction pairs, they were cleaned by ultrasonication in petroleum ether before testing. The volume of the lubricant used in tribological tests was 0.2 mL. The lubricant was added to the contact surface of the fiction pairs as droplets with a pipette to form a continuous lubricating layer covering the entire wear track area. The coefficient of friction (COF) *versus* sliding time curves were recorded automatically and timely, and at least three repeated measurements for each test condition were conducted.

The friction properties of the lubricant mixed with rGO/ZrO_2 composite were strongly influenced by its concentrations. The experiments for determining optimum concentrations have been tested with a constant load of 50 N for 30 min to obtain the best lubricating performance. For comparison, the pure oil and oil separately mixed with natural graphite powders, ZrO_2 nanoparticles, rGO nanosheets and commercial zinc dialkyl dithiophosphate (ZDDP) at the optimum concentration were also studied under the same conditions. After performing the friction testing using various materials as lubricant additives, the resulting wear tracks were observed by scanning electron microscopy (SEM) using a JSM-5600LV scanning electron microscope. Wear scars of the ball were measured by an Olympus STM6 microscope (Japan). The wear volume and the height profile of the tracks were obtained with a noncontact 3D surface profiler (model MicroMAXTM, ADE, USA). The wear rate (K) of the discs was calculated according to the formula below:

$$K = \frac{V}{F \cdot \mathrm{d}}$$

Where V (μm^3) is the volume loss, which can be measured with a MicroMAXTM non-contact 3D surface profiler, F (N) represents the loading force which is a constant load of 50 N while d (m) represents the sliding distance which is also a constant of 1 mm under the our experimental conditions.

3. Results and Discussion

3.1 Characterizations of the as-prepared rGO/ZrO_2 nanocomposites

To obtain the best distributed sample, TEM images of the prepared rGO/ZrO_2 nanocomposites obtained by various volume ratios of GO to $ZrOCl_2$ solutions are compared in Fig. 1. As shown in Fig. 1a~g, the morphology of composites is uneven distribution when the proportion of $ZrOCl_2$ solution in mixture possesses too high or too low. In particular, the pure rGO nanosheets present highly wrinkled (Fig. 1a) and ZrO_2 nanoparticles are also severely agglomerated (Fig. 1g), and the as-prepared rGO nanosheets are thin with a clearly corrugated structure in good agreement with the atomic force microscope (AFM) observation in Electronic Supporting Information (ESI†) Fig. S1, which further confirms that the large sheets of rGO are a stack of few layers. The reason is that rGO nanosheets gradually aggregated and formed the stacked graphite structure due to their high specific surface in the process of their dispersion[23]. However, when the volume ratio of GO to $ZrOCl_2$ solution was set as 2:1, ZrO_2 nanoparticles anchored onto rGO are homogeneous and moderate, meanwhile, rGO nanosheets remain flat and no obviously curled sheets observed (Fig. 1d). Moreover, the lattice spacing of 0.296 nm displayed in HRTEM image (Fig. 1h) is consistent with the (111) plane of the tetragonal structure ZrO_2, in which the size of

about 5 nm is in accordance with the calculated value based on XRD results shown in Fig. 2a. Besides, the selected area electron diffraction (SAED) pattern displays that the position of detectable rings are equivalent to lattice positions from standard tetragonal ZrO_2 (JCPDS PDF No. 49-1642). The well dispersed structure of the composite suggested that ZrO_2 nanoparticles could act as spacers preventing the rGO from restacking and thus increased the stability of the exfoliated rGO nanosheets[24], and reduced the surface energy of each other and the agglomeration phenomenon was effectively prevented[25]. Therefore, the optimal composite sample (GO to $ZrOCl_2$/(v:v)=2:1) was chosen for the following characterizations.

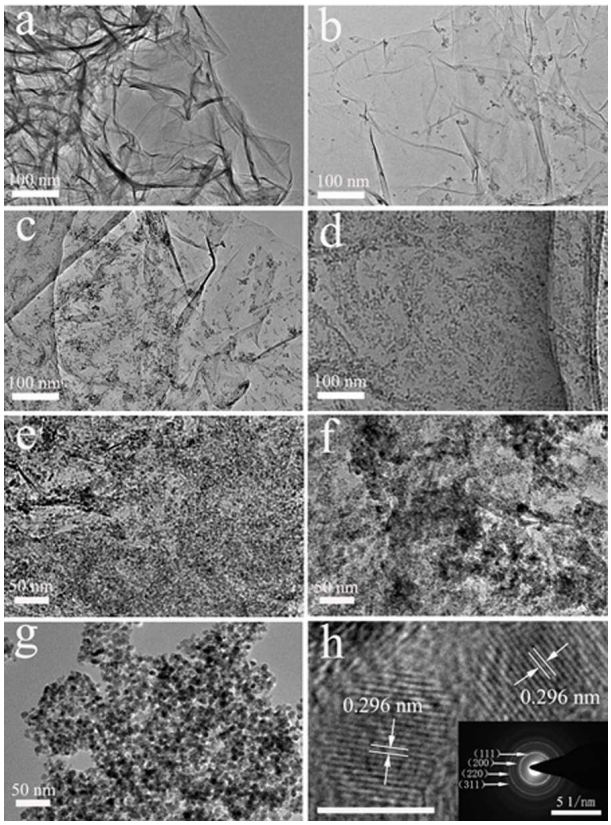

Fig. 1 TEM images of rGO/ZrO_2 nanocomposites obtained by various volume ratios of GO to $ZrOCl_2$ solutions: (a) 1:0, (b) 5:1, (c) 3:1, (d) 2:1, (e) 1:1, (f) 1:2, (g) 0:1, (h) HRTEM image of (d). The inset in (h) provides the SAED pattern of the composite.

Fig. 2a presents the XRD patterns of the prepared rGO/ZrO_2 nanocomposite and the control samples. Obviously, the pattern of rGO presents a broad diffraction peaks at 22.4° (d ≈ 0.386 nm), suggesting the hydrothermal reduction allowed the rGO nanosheets to tightly pack[26]. The crystal structure of ZrO_2 nanoparticles exists with the tetragonal and monoclinic, in good agreement with standard cards (JCPDS PDF No. 49-1642) and (JCPDS PDF No. 37-1484), respectively, but the former has a distinct advantage of the relative intensity and the peak of quantity. Moreover, the average size of the ZrO_2 nanoparticles calculated by the Debye-Scherrer formula is about 5 nm. The rGO/ZrO_2 nanocomposite shows characteristic peaks of rGO (002) and ZrO_2 of tetragonal structure, indicating the presence of ZrO_2 nanoparticles over rGO nanosheets.

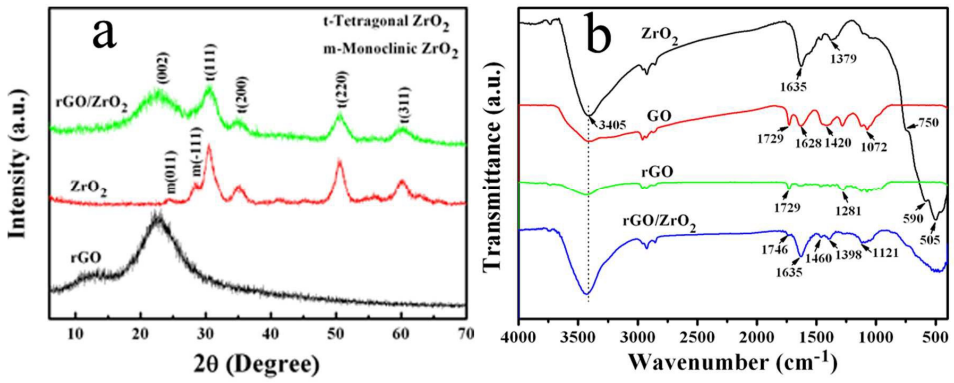

Fig. 2 (a) XRD patterns of synthetic rGO, ZrO_2 and rGO/ZrO_2 nanocomposite; (b) FTIR spectra of synthetic ZrO_2, GO, rGO, rGO/ZrO_2 nanocomposite. (A color version of this figure can be viewed online)

FTIR spectra of ZrO_2, GO, rGO and rGO/ZrO_2 nanocomposite are shown in

Figure 2b. Obviously, a broad peak at ~3405 cm^{-1} attributed to O-H stretching vibration of adsorbed water molecule appears in all samples. The FTIR spectrum of ZrO_2 displays some peaks at 1635 cm^{-1} (O-H bending vibration of water molecule), 750 cm^{-1}, 590 cm^{-1} and 505 cm^{-1} (Zr-O stretching vibrations)[27,28]. The spectrum of GO presents the typical peaks at 1729 cm^{-1} (C=O stretching vibration of -COOH and C=O), 1629 cm^{-1} (C=C skeleton stretching vibration and O-H bending vibration of water molecule), 1420 cm^{-1} (O-H bending vibration of -COOH and C-OH), 1281 cm^{-1} (C-O stretching vibration of phenols and ethers and epoxy group), 1121 cm^{-1} (C-O-C stretching vibration), and 1072 cm^{-1} (C-O stretching vibration of -OH)[29,30]. For rGO, the peaks of containing-oxygen groups corresponding to GO are mostly weakened and slightly disappeared, indicating that GO was reduced incompletely. However, for rGO/ZrO_2 nanocomposite, the characteristic peak of the C=O stretching vibration is shifted from 1729 to 1746 cm^{-1}, which is attributed to the influence of coordination between O and Zr on the surface of ZrO_2 nanoparticles[38], and the relative intensity decreases significantly. What's more, the broad peak at 1420 cm^{-1} has separated into two small peaks at 1460 and 1398 cm^{-1}, which can be assigned to the formation of either monodentate complex or bidentate complex between the oxygen-containing groups of GO and Zr(IV) from the hydrolysis of $ZrOCl_2$ solution[31,32]. So, it can be concluded that the ZrO_2 nanoparticles are fully bonded onto the surface of rGO nanosheets.

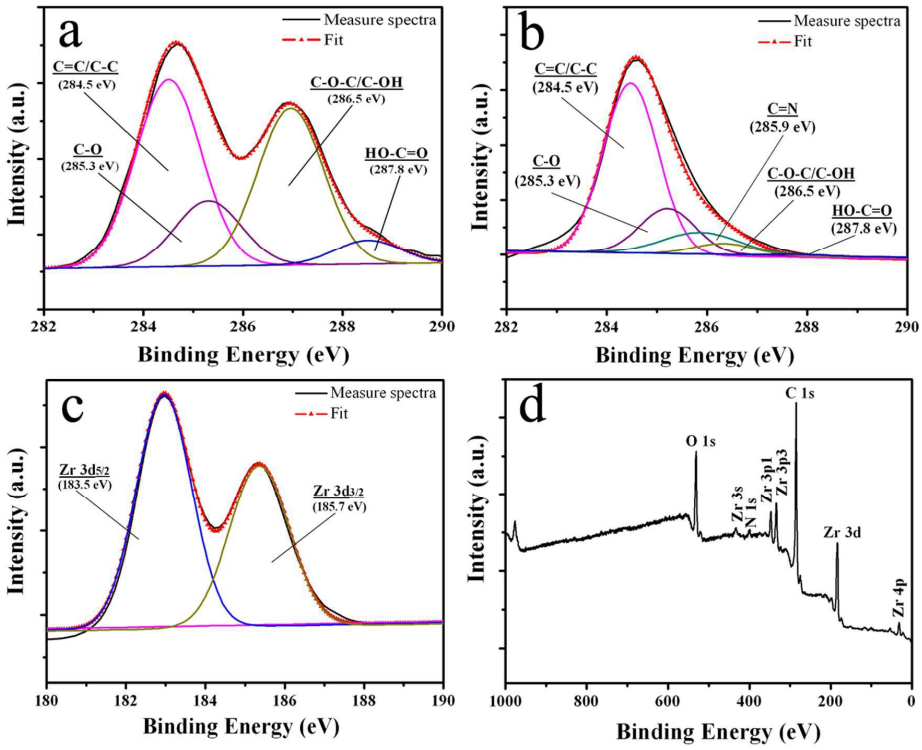

Fig. 3 (a) XPS spectrum of the C 1s for GO nanosheets; (b) The C 1s spectrum and (c) Zr 3d spectrum for rGO/ZrO_2 nanocomposite; and (d) the corresponding XPS survey spectrum. (A color version of this figure can be viewed online)

Fig. 3 provides the XPS analyses of GO and rGO/ZrO_2 nanocomposite to confirm the chemical changes. As shown in Fig. 3a, the C 1s XPS spectrum of GO unambiguously indicates a considerable degree of oxidation with four kinds of carbon atoms coming from the different functional groups: the non-oxygenated ring C (C=C/C-C, 284.5 eV), the C in C-O bonds (285.3 eV), the C in O-C-O/C-OH (286.5eV), and the C in HO-C=O (287.8 eV)[33]. In Fig. 4b, the C 1s XPS spectrum of the rGO/ZrO_2 also exhibits the same oxygen functionalities corresponding to the GO nanosheets, but the peak intensities of these components are much weaker than those

in the GO, proving considerable deoxygenation by the reduction process. In addition, the presence of an additional component at 285.6 eV corresponding to the C in C=N bond of hydrazine[34] is in good agreement with XPS survey spectrum of rGO/ZrO_2 nanocomposite shown in Fig. 3d. These observations suggest GO was deoxygenated by the hydrothermal process and nitrogen incorporation. In Fig. 4c, the binding energies of Zr $3d_{5/2}$ and Zr $3d_{3/2}$ are 183.5 and 185.7 eV, respectively, indicating zirconium was oxidized into its Zr^{4+} state[35].

All characterizations clearly confirmed that ZrO_2 nanoparticles have been successfully anchored onto rGO sheets. The synthesis process of rGO/ZrO_2 nanocomposite is schematically illustrated in Fig. 4. When the $ZrOCl_2$ solution was mixed with GO, the wealthy negative charges and the abundant oxygen-containing functional groups at the surface and edges of GO nanosheets can attract and strongly bond with Zr(IV) complex ions coming from the hydrolysis of $ZrOCl_2$ precursor, such as $\left[Zr(OH)_2 \cdot 4H_2O\right]_4^{8+}$ and $\left[Zr(OH)_{2+x} \cdot (4-x)H_2O\right]_4^{(8-4x)+}$ [36, 37], which might be physically or chemically absorbed onto GO nanosheets. Subsequently, as the whole reaction carries out, Zr(IV) complex ions transformed into stable ZrO_2 nanoparticles by nucleation and further growth, meanwhile, GO nanosheets were reduced into rGO under the experimental conditions of high temperature and pressure as well as the presence of hydrazine hydrate with excessive alkali. Finally, ZrO_2 nanoparticles were grown uniformly onto rGO nanosheets to form the composites.

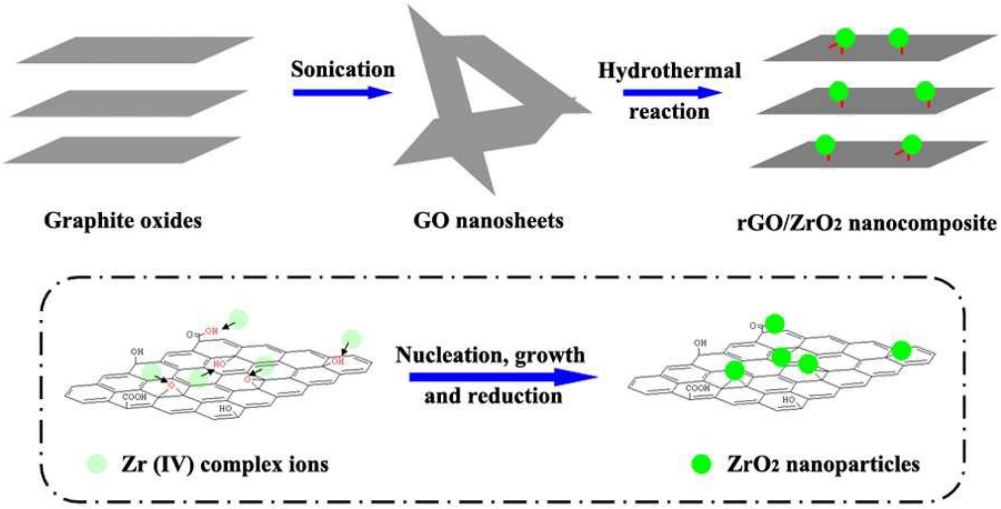

Fig. 4 A sketch showing the preparation process of rGO/ZrO_2 nanocomposite. The inset shows the specific integrating process occurring in hydrothermal reaction. (A color version of this figure can be viewed online)

3.2 Dispersible stability of rGO/ZrO_2 nanocomposite in paraffin oil

In Fig. 5, the dispersion stability of ZrO_2, graphite, rGO and rGO/ZrO_2 nanocomposite in paraffin oil were evaluated and compared using the same method. According to the sedimentation curves of different samples ultrasonically dispersed in pure oil (Fig. 5a), the sedimentation rate that the relative concentration of samples in oil changes with the settled time is obvious, in particular, the sedimentation of the ZrO_2 and graphite is remarkably fast. Further, after a long period of settling time (240 min), the relative concentration of the composite is mantained at ~0.93 much higher than the relative concentration of ~0.76 for rGO. As shown in Fig.5b, the change is consistent with the optical signal of different samples dispersed in the pure oil at different settling times. At first, the different samples were well-dispersed in the pure

oil after sonication. After being settled for 48 h, the lubricants containing additives except rGO/ZrO_2 nanocomposite occurred obvious precipitation, in other words, rGO/ZrO_2 nanocomposite was still homogeneously dispersed in the oil. Therefore, the photos and sedimentation curves of different samples illustrated that the dispersion stability of graphene in paraffin oil could be improved by the surface modification with inorganic nanoparticles and the way is effective; similarly, the effectiveness was confirmed by the modification of graphene using cerium oxide [38].

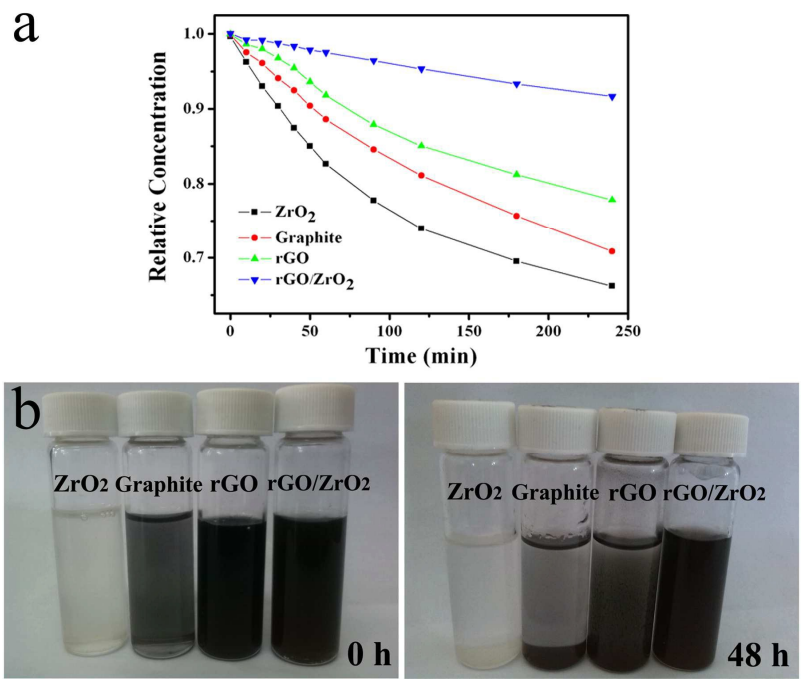

Fig. 5 (a) Dispersion stabilities of the pure oil containing ZrO_2, graphite, rGO and rGO/ZrO_2 determined by UV-vis spectraphotometry. (b) Optical photos of above samples dispersed in pure oil at different settling times. (A color version of this figure can be viewed online)

3.3 Tribological properties of rGO/ZrO_2 nanocomposite as lubricant additives

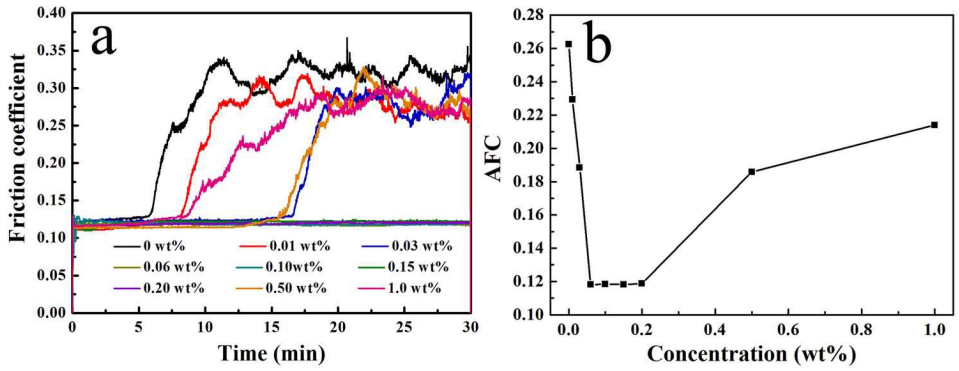

Fig. 6 (a) COF of oil containing different concentrations of rGO/ZrO_2 nanocomposite as a function of time and (b) the corresponding average friction coefficient (AFC) as a function of concentration. (A color version of this figure can be viewed online.)

To study the concentration influence of rGO/ZrO_2 on lubricating properties of paraffin oil, several concentrations of oil mixed with the prepared composite were tested at a constant load of 50 N for 30 min. As shown in Fig. 6a, COF rose suddenly after about 6 min under the test with the pure oil, which could be ascribed to the fracture of oil film. However, the stability time of COF for the base oil had significant improvement after mixing with a small amount of nanocomposite (0.01 wt% and 0.03 wt%). Obviously, it can be seen that the effective concentration presented a wider range of 0.06 wt% ~ 0.2 wt% with the same average friction coefficient (AFC) value of about 0.118 (in Fig. 6b), far below the AFC value of 0.263 for the pure oil. Further, the stability time of COF for the base oil mixed with the composite was shorten when its concentration in paraffin oil increased up to over 0.2 wt%, indicating that the dispersions were not completely stable throughout the test due to the inhomogeneous lubricant caused by agglomeration[39]. It can be concluded that the lubricating

property of oil containing the right amount of rGO/ZrO_2 nanocomposite does not decrease, and the lubricating oil film formed on friction surface is strong enough to support the sliding shear stress. Based on the COF observations of various concentrations of rGO/ZrO_2 nanocomposite in pure oil, the effective concentration of 0.06 wt% was chosen for the following testing.

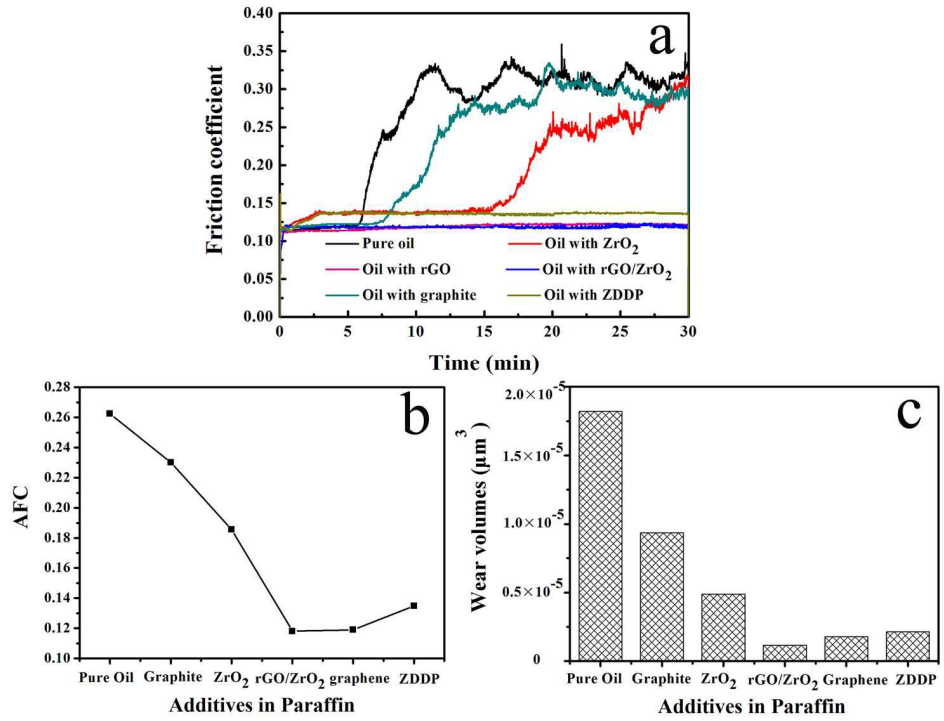

Fig. 7 COF of rGO/ZrO_2 nanocomposite and the control samples dispersed in pure oil (0.06 wt%) (a) as a function of time and the corresopnding (b) AFC and (c) the wear volumes of wear tracks on the disc. (A color version of this figure can be viewed online)

For comparison, Fig. 7 presents COF and the corresopnding AFC as well as wear volumes of wear tracks on the discs for pure oil, oil containing rGO/ZrO_2 and the control samples at the same concentration of 0.06 wt%. Moreover, the corresponding

mean area of wear scars for steel ball, and the wear rates of wear tracks on the discs were calculated and summarized in Table 1. As shown in Fig. 7a, the stability property of COF for oil containing rGO/ZrO_2 nanocomposite and rGO nanosheets was similar, smaller and more stable than the pure oil, oil with graphite, ZrO_2 and ZDDP (the commercial and frequently used an additive). In Fig. 7b, AFC value of the pure oil is about 0.263, much higher than others. In all testing samples, the AFC value of 0.118 for the oil mixed with rGO/ZrO_2 nanocomposite is lowest and is also closer to the AFC value of 0.119 for the oil mixed with rGO nanosheets. In Fig. 7c, the wear volume (1.820×10^5 μm^3) and wear rate (33.70 $\mu m^3/N\cdot m$) in Table 1 are the maximum for the test of pure oil. Moreover, the addition of ZrO_2 nanoparticles has no obvious effect on the reduction of the COF for the pure oil, but it can increase the micro-hardness of the oil film formed between the friction pairs and thus improve the wear resistance of the oil film[40]. Obviously, the wear volume of 0.116×10^5 μm^3 and the wear rate of 2.15 $\mu m^3/N\cdot m$ for the oil containing rGO/ZrO_2 nanocomposite are lower than the values of the wear volume of 0.177×10^5 μm^3 and the wear rate of 3.28 $\mu m^3/N\cdot m$ for the oil containing rGO nanosheets, and are also lowest in all testing samples.

By comparison, it can be concluded that the lubricant containing various additives can reduce the wear in different degree. Thereinto, the oil containing the rGO/ZrO_2 nanocomposite presents the optimal tribological properties; namely, AFC reduced from 0.263 to 0.118 and the wear rate reduce to 6.4% of pure oil, which can be attributed to the fact that the unique layered structure and small size of rGO/ZrO_2

nanocomposite are convenient for entering the interfaces of the friction pairs, and also easy shearing under the tribo-stressed zone due to the weakly Van der Waals interaction between their coordinated lamellas. Besides, the oil containing rGO/ZrO_2 nanocomposite has a high load-bearing capacity preventing the oil film from the fracture, and the good dispersion stability of the composite in oil ensures their continuous supply on the tribological interfaces during test.

Table 1 The mean area of wear scars of steel balls, wear volumes and Wear rates of the discs for all six cases

Test conditions	The mean area of wear scars on balls (μm^2)	Wear volumes on discs (μm^3)	Wear rates on discs ($\mu m^3/N \cdot m$)
Pure oil	1.922×10^5	1.820×10^5	33.70
Oil with graphite	1.627×10^5	0.935×10^5	17.31
Oil with ZrO_2	1.339×10^5	0.487×10^5	9.02
Oil with rGO/ZrO_2	0.452×10^5	0.116×10^5	2.15
Oil with rGO	0.461×10^5	0.177×10^5	3.28
Oil with ZDDP	0.565×10^5	0.214×10^5	3.96

After friction testing, the micrographs and wear depths of the different worn tracks characterized by the measurements of OM, SEM and 3D surface profiler were displayed in Fig. 8. As shown in Fig. $8a_1$-a_3, for the test performed with pure oil alone, the worn surfaces are the roughest with severe scuffing signs as well as the wide and deep grooves, and the mean area of worn scar on ball is also the largest (1.922×10^5

μm^2) in Table 1, which indicates that the boundary lubricating film at the contact surfaces has poor strength. By contrast, all additives used in our experiments can reduce wear to some extent, but the anti-wear ability is different. The additives of ZrO_2 and graphite have the poor wear resistance so that the worn tracks are rough and the mean area of worn scars on ball are large, although they are lower than that of the pure oil. It is attributed to the fact that the agglomerate blocks of ZrO_2 nanoparticles act as abrasive particles and increase the roughness of oil film, while the lubricating oil film containing graphite fractures and loses efficacy eventually. For the test performed with ZDDP, the tribological properties are better than the above two kinds of additives, attributing to the good lubricating property and load-bearing capacity. Apparently, the worn surfaces seem to be uniform and smooth, and the mean area of worn scar on ball is the minimum (0.452×10^5 μm^2) in all testing samples for the oil containing rGO/ZrO_2 nanocomposite (in Fig. 8d_1-d_3). The results suggested that a good surface protective film formed on the frictional interfaces, which is in agreement with the low COF for the oil mixed with the composite. Furthermore, the rGO is also effective in reducing wear but is inferior to the as-prepared composite.

To further testify whether the tribological properties of the oil mixed with the prepared composite are better than those of the oil mixed with the rGO nanosheets, two experiments were performed under the high load as shown in Fig. 9. In Fig. 9a, the results displayed that COF in sequence rose for the pure oil and oil containing rGO nanosheets after being tested for about 4 and 7 min under the constant load of 100 N, respectively. However, COF for the oil containing rGO/ZrO_2 nanocomposite is

stable and low in the whole test process. What's more, the maximum load-bearing capacity of the oil containing the composite could be elevated up to 450 N, although the COF gradually increased after being tested for 15 min at this load (Fig. 9b).

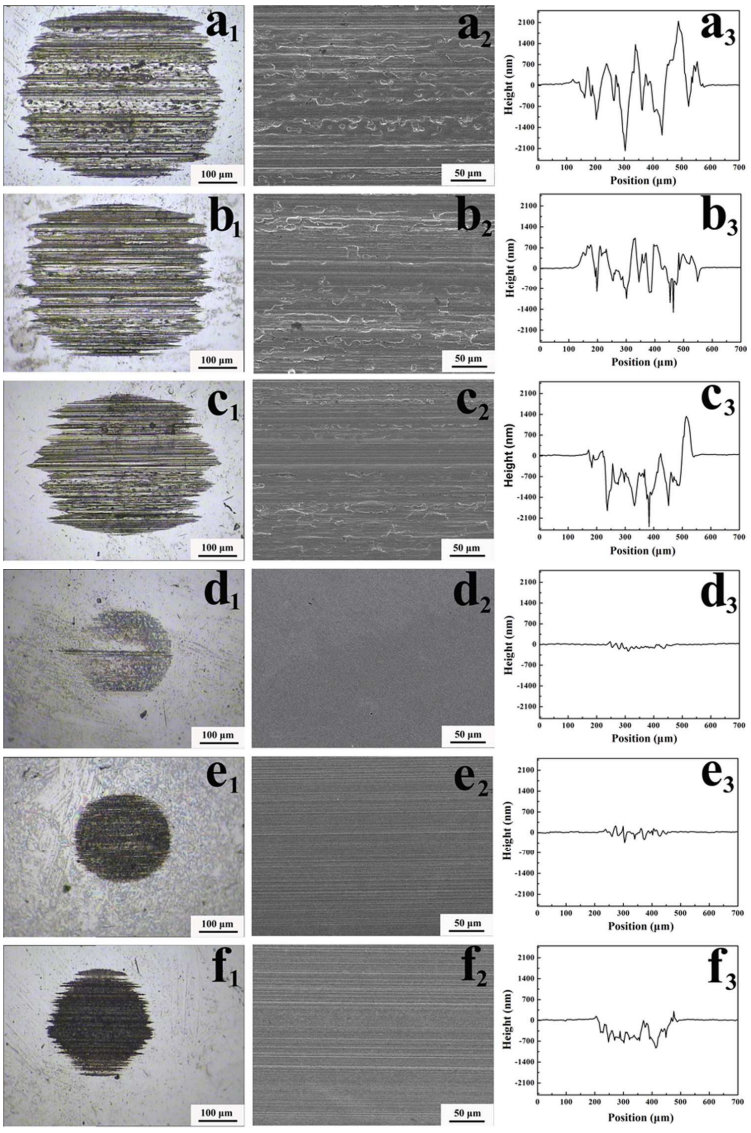

Fig. 8 Optical images of the wear surfaces on the balls, SEM micrographs and height profile measurements of the tracks on the counter discs after the friction test for 30 min at 50 N. Lubricated with pure oil (a), graphite (b), ZrO_2 (c), rGO/ZrO_2 (d), rGO (e) and ZDDP (f) dispersed in the pure oil (0.06 wt%), respectively.

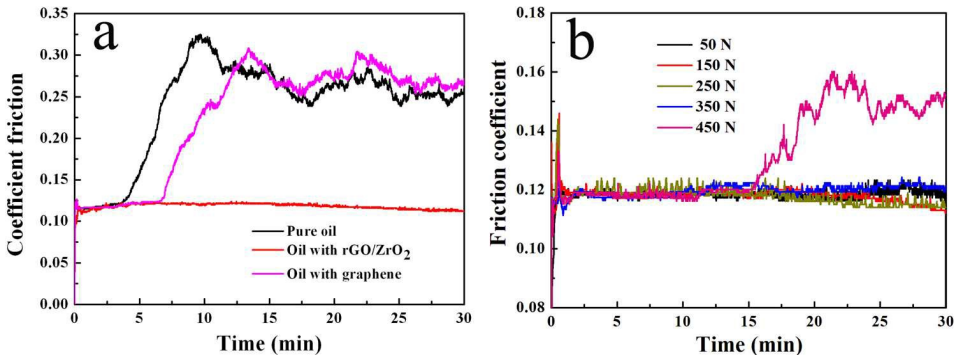

Fig. 9 Variations of friction coefficients with time for the oil mixed with rGO/ZrO_2 nanocomposite and the control samples at the concentration of 0.06 wt% (a) under a constant load of 100 N (b) under a series of constant high load. (A color version of this figure can be viewed online.)

Based on the above research, the excellent tribological properties of the as-prepared rGO/ZrO_2 nanocomposite acting as a novel additive in paraffin have been proved. The tribological model of the rGO/ZrO_2 nanocomposite in paraffin oil is vividly depicted in Fig. 10. The possible lubricating mechanism can be described as follows: firstly, because the ZrO_2 nanoparticles anchored onto rGO nanosheets cover up the nanogaps of the rubbing surfaces, preventing the direct contact from friction pairs under contact stress. Moreover, the lamellar structure of rGO nanosheets forms a conformal protective film between the contact interfaces under the friction stress, it can provide the low resistance for shear and thus result in the reductions of the friction and wear[41]**.** Similarly, such finding was also supported by a formation of a MoS_2 transfer film in the contact area, because the structure of MoS_2 is similar to that of the graphene[42]. In addition, the presence of ZrO_2 nanoparticles on the surface of

rGO nanosheets can act as bearing contributing to resist wear and improve the capacity of load-bearing for lubricant[43]. The excellent lubricating properties support that the as-prepared composite is a kind of the potential candidates as lubricant additive in tribology.

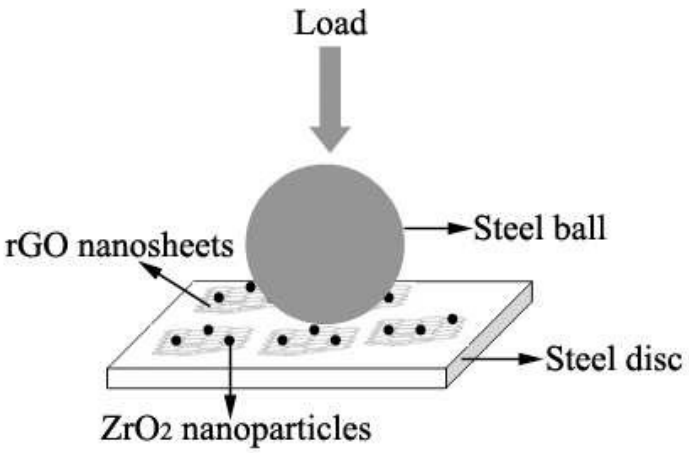

Fig. 10 The tribological model of the rGO/ZrO_2 nanocomposite in paraffin oil.

4. Conclusions

By the one-pot hydrothermal method, we have successfully synthesized the uniformly distributed rGO/ZrO_2 nanocomposite by adjusting the precursor proportion of GO colloidal suspension and $ZrOCl_2$ solution. The combination process of ZrO_2 nanoparticles with rGO nanosheets might be described as follows: the positively charged Zr(IV) complex ions coming from the hydrolysis of $ZrOCl_2$ solution are adsorbed onto the surface of negatively charged GO nanosheets by electrostatic attraction, then through nucleation, further growth and reduction during hydrothermal reaction, finally, nanocomposite of rGO/ZrO_2 is formed. As a novel lubricant additive, the as-prepared rGO/ZrO_2 nanocomposite has the good dispersion stability

in paraffin oil, but also presents the excellent friction-reduction and anti-wear properties, which can be attributed to the following facts that ZrO_2 nanoparticles acting as spacers and avoiding the restacking of rGO nanosheets, as well as the synergetic effect of lubricating property from lamellar structure of rGO and bearing property of ZrO_2. Upon the test with the oil containing the composite with a concentration of 0.06 wt%, the results showed an excellent tribological properties, namely, AFC reduced from 0.263 to 0.118 and the wear rate reduced to 6.4% of pure oil as well as the load-bearing capacity improved tremendously up to 450 N. Above results suggest that the prepared rGO/ZrO_2 nanocomposite is a potential candidate of lubricant additives to improve the tribological properties of oil based lubricants.

Acknowledgements

This work has been supported by the National Natural Science Foundation of China (Grant Nos. 51205385 and 51375474), the "Funds for Young Scientists of Gansu Province (145RJYA280)", and the open foundation of the State Key Laboratory of Solid Lubrication at LICP (LSL-1209).

Notes and references

[1] X. W. Pei, L. T. Hu, W. M. Liu and J. C. Hao, *Eur. Polym. J.*, 2008, **44**, 2458–2464.

[2] S. E. Campbell, G. Luengo, V. I. Srdanov, F. Wudi and J. N. Israelachvili, *Nature*, 1996, **382**, 520–522.

[3] K. S. Novoselov, A. K. Geim, S. V. Morozov, D. Jiang, Y. Zhang, S. V. Dubonos, I. V. Grigorieva and A. A. Firsov, *Science*, 2004, **306**, 666–669.

[4] A. K. Geim, *Science*, 2009, **324**, 1530–1534.

[5] Y. Zhu, S. Murali, W. Cai, X. Li, J. W. Suk, J. R. Potts and R. S. Ruoff, *Adv. Mater.*, 2010, **22**, 3906–3924.

[6] J. Robertson, *Mater. Today*, 2004, **7**, 46–52.

[7] Y. W. Gao and P. Hao, *Physica E*, 2009, **41**, 1561–1566.

[8] V. Eswaraiah, V. Sankaranarayanan and S. Ramaprabhu, *ACS Appl. Mater. Interfaces*, 2011, **3**, 4221–4227.

[9] L. Y. Lin, D. E. Kim, W. K. Kim and S. C. Jun, *Surf. Coat. Technol.*, 2011, **205**, 4864–4869.

[10] M. D. Stoller, S. Park, Y. Zhu, J. An and R. S. Ruoff, *Nano Lett.*, 2008, **8**, 3498–3502.

[11] O. Elomaa, V. K. Singh, A. Lyer, T. J. Hakala and J. Koskinen, *Diamond Relat. Mater.*, 2015, **52**, 43–48.

[12] D. Berman, A. Erdemir and A. V. Sumant, *Carbon*, 2013, **59**, 167–175.

[13] H. P. Mungse, N. Kumar and O. P. Khatri, *RSC Adv.*, 2015, **5**, 25565–25571.

[14] C. Lee, X. Wei, J. W. Kysar and J. Hone, *Science*, 2008, **321**, 385–388.

[15] J. H. Ouyang and S. Sasaki, *Ceram. Int.*, 2001, **27**, 251–260.

[16] S. C. Moulzolf, R. J. Lad and P. J. Blau, *Thin Solid Films*, 1999, **347**, 220–225.

[17] J. Wang, S. Yang, X. Liu, S. Ren, F. Guan and M. Chen, *Appl. Surf. Sci.*, 2004, **221**, 272–280.

[18] S. M. Kwon, S. J. Lee and I. J. Shon, *Ceram. Int.*, 2015, **41**, 835–842.

[19] P. A. K. Rao, S. Singh, B. R. Singh, W. Khan and A. H. Naqvi, *J. Environ. Chem.*

Eng., 2014, **2**, 199–210.

[20] H. Teymourian, A. Salimi, S. Firoozi, A. Korani and S. Soltanian, *Electrochim. Acta*, 2014, **143**, 196–206.

[21] H. Q. Li, Y. T. Xie, K. Li, L. P. Wang and X. B. Zheng et al, *Ceram. Int.*, 2014, **40**, 12821–12829.

[22] Y. Xu, H. Bai, G. Lu, C. Li and G. Shi. *J. Am. Chem. Soc.*, 2008, **130**, 5856–5857.

[23] H. J. Song, X. H. Jia, N. Li, X. F. Yang and H. Tang, *J. Mater. Chem.*, 2012, **22**, 895–902.

[24] Z. S. Wu, D. W. Wang, W. C. Ren, J. P. Zhao, G. G. Zhou, F. Li and H. M. Cheng, *Adv. Funct. Mater.*, 2010, **20**, 3595–3602.

[25] Y. Zhang, H. Tang, X. R. Ji, C. S. Li, L. Chen, D. Zhang, X. F. Yang and H. T. Zhang, *RSC Adv.*, 2013, **3**, 26086–26093.

[26] S. Park, J. An, I. Jung, R. D. Piner, S. J. An, X. Li, A. Velamakanni and R. S. Ruoff, *Nano Lett.*, 2009, **9**, 1593–1597.

[27] S. K. Maity, M. S. Rana, B.N. Srinivas, S. K. Bej, G. M. Dhar and T. S. R. Prasada Rao, *J. Mol. Catal. A-Chem.*, 2000, **153**, 121–127.

[28] S. F. Wang, F. Gu, M. K. Lü, Z. S. Yang, G. J. Zhou, H. P. Zhang, Y. Y. Zhou and S. M. Wang, *Opt. Mater.*, 2006, **28**, 1222–1226.

[29] M. Acik, G. Lee, C. Mattevi, A. Pirkle, R. M. Wallace, M. Chhowalla, K. Cho and Y. Chabal, *J. Phys. Chem. C*, 2011, **115**, 19761–19781.

[30] H. P. Mungse and O. P. Khatri, *J. Phys. Chem. C*, 2014, **118**, 14394–14402.

[31] Q. Huang and L. Gao, *J. Mater. Chem.*, 2003, **13**, 1517–1519.

[32] H. J. Song, X. H. Jia, N. Li, X. F. Yang and H. Tang, *J. Mater. Chem.*, 2012, **22**, 895–902.

[33] S. Stankovich, R. D. Piner, X. Q. Chen, N. Q. Wu, S. B. T Nguyen and R. S. Ruoff, *J. Mater. Chem.*, 2006, **16**, 155–158.

[34] R. J. Waltman, J. Pacansky and C.W. Bates Jr., *Chem. Mater.*, 1993, **5**, 1799–1804.

[35] XPS Handbook of the Elements and Native Oxides, XPS International Inc, 1999 (http:www.xpsdata. com/PDF/zr-no.pdf).

[36] K. Matsui and M. Ohgai, *J. Am. Ceram. Soc.,* 2001, **84**, 2303–2312.

[37] K. Matsui and M. Ohgai, *J. Am. Ceram. Soc.,* 2000, **83**, 1386–1392.

[38] G. Y. Bai, J. Q. Wang, Z. G. Yang, H. G. Wang, Z. F. Wang and S. R. Yang, *RSC Adv.*, 2014, **4**, 47096–47105.

[39] V. K. Singh, O. Elomaa, L. S. Johansson, S. P. Hannula and J. Koskinen, *Carbon*, 2014, **79**, 227–235.

[40] S. Sharma, *Int. J. Adv. Des. Manuf. Technol.*, 2012, **61**, 889–900.

[41] D. Berman; A. Erdemir and A. V. Sumant, *Carbon*, 2013, **54**, 454–459.

[42] M. Praveena; C. D. Bain; V. Jayaram and S. K. Biswas, *RSC Adv.*, 2013, **3**, 5401–5411.

[43] V. K. Singh, O. Elomaa, L. S. Johansson, S. P. Hannula and J. Koskinen, *Carbon*, 2014, **79**, 227–235.